Smith Benjamin P. (Orcid ID: 0000-0003-3189-8717)
Ingalls Miquela (Orcid ID: 0000-0002-7451-2944)
Trower Elizabeth J. (Orcid ID: 0000-0001-9898-5589)
Present Theodore Michael (Orcid ID: 0000-0002-4747-2174)
Magyar John S. (Orcid ID: 0000-0002-3586-8286)

Physical Controls on Carbonate Intraclasts: Modern Flat Pebbles from Great Salt Lake, Utah

B. P. Smith[1], M. Ingalls[1,2], E.J. Trower[3], U. F. Lingappa[1], T. M. Present[1], J. S. Magyar[1], and W.W. Fischer[1]

[1]Division of Geological and Planetary Sciences, California Institute of Technology, Pasadena, CA, 91125, USA.

[2]Department of Geosciences, The Pennsylvania State University, University Park, Pennsylvania 16802, USA.

[3]Department of Geological Sciences, University of Colorado Boulder, Boulder, Colorado 80309, USA.

Corresponding author: Ben Smith (bpsmith@caltech.edu)

Key Points:

- Sediment cohesion within carbonate environments depends on both physical and chemical energy near the sediment-water interface.
- If sediment transport is infrequent, burrowing animals provide a significant source of physical energy
- Substrate cohesion may record physical changes related to the number and behavior of animals rather than geochemical conditions.

This article has been accepted for publication and undergone full peer review but has not been through the copyediting, typesetting, pagination and proofreading process which may lead to differences between this version and the Version of Record. Please cite this article as doi: 10.1029/2020JF005733

Abstract

In carbonate-forming environments, authigenic minerals can cement surface sediments into centimeter-sized intraclasts that are later reworked into “flat-pebble” or “edgewise” conglomerates. Flat-pebble conglomerates comprise only a small portion of facies in modern marine environments but are common in ancient strata, implying that seafloor cements were more widespread in the past. Flat-pebble conglomerates nearly disappeared after the Ordovician radiation, yet it is unclear if this decline was due to changing seawater chemistry or if increased infaunalization and bioturbation simply worked to break down nascent clasts.

We discovered a process analog that produces flat-pebble conglomerates around the Great Salt Lake, Utah, USA—and studied these facies using field observations, wave models, satellite imagery, petrography, and microanalytic chemical data. Clasts were sourced from wave-rippled grainstone that cemented *in situ* in offshore environments. Lake floor cements formed under aragonite saturation states that are lower than modern marine settings, suggesting that physical processes are at least as important as chemical ones. Results from our wave models showed that coarse sediments near the field site experience quiescent periods of up to six months between suspension events, allowing isopachous cements to form. Using a simple mathematical framework, we show that the main difference between Great Salt Lake and modern, low-energy marine settings is that the latter has enough bioturbating organisms to break up clasts. Observations from Great Salt Lake demonstrate how geologic trends in flat-pebble abundance could largely reflect changes in total infaunal biomass and ecology without requiring regional-to-global changes in seawater chemistry.

Plain Language Summary

Calcium carbonate is a common sedimentary mineral that precipitates quickly under Earth surface conditions. If carbonate sediments are at rest for long periods of time they may solidify via cementation into flat, pebble-sized clasts. Geologic trends show that flat pebbles are anti-correlated with burrows, suggesting they may tell us about animal evolution and ecology. However, it was unknown if animals disrupt clasts through chemical means, leading to slower rates of mineral growth, or if they physically push sediments apart, breaking up nascent cements. We studied flat pebbles forming in Great Salt Lake, Utah, where the water is too salty for burrowing animals. The composition of lake water should lead to slower growth rates for carbonate minerals, yet clasts still form. We conclude that pebbles form during quiescent intervals with little physical energy to move grains, either from waves or from burrowing organisms. As a result, ancient flat pebbles are probably not unique markers for seawater chemistry.

1 Introduction

The degree of cohesion among seafloor sediments has changed drastically over Earth history. Modern substrates are typically loosely bound, yet some ancient carbonate facies imply greater cohesion in the past. The occurrence of facies such as stromatolites, molar-tooth structures, and seafloor crystal fans in Precambrian strata shows that mineral growth and microbial biofilm contributed to widespread early lithification in early Earth history (Cantine et al., 2020; Grotzinger & James, 2000). Early Paleozoic animals, however, reduced sediment cohesion through their feeding and burrowing activities (Droser & Bottjer, 1989; Thayer, 1979). As a result, shallow marine sedimentology often tracks changes in animal behaviors introduced during major radiations and extinctions. One well-known example is that of flat-pebble conglomerates—a type of intraformational conglomerate/breccia comprised of platy clasts formed when storms ripped apart cohesive sediment substrates (Sepkoski, 1982). Flat-

pebble deposits vanished after mid-Ordovician time, coincident with a major increase in burrow depth and intensity (Droser & Bottjer, 1989; Sepkoski, 1982). Younger examples of flat-pebble conglomerates were deposited during time periods associated with biomass reductions after mass extinctions and were particularly common in unburrowed Early Triassic sediments (Payne et al., 2006; Pruss et al., 2005; Wignall & Twitchett, 1999).

If flat pebbles formed under a narrow set of biological and chemical conditions, then they should constrain changes in ocean basins during both Precambrian time and upheavals in Phanerozoic biodiversity. In his seminal work on flat pebbles, Sepkoski (1982) outlined two ways in which animal-sediment interactions might suppress sediment cohesion. The first explanation involves the physical transfer of energy by organisms. Burrowing organisms expend some of their metabolic energy as external work that moves sedimentary particles (Dorgan et al., 2011) and large, highly motile, or densely packed infaunal metazoans could break up carbonate cements before they form clasts (Sepkoski, 1982). Under this hypothesis, the mechanical energy transferred to sediments by bioturbating organisms may be significant, particularly in environments where sediment transport is infrequent. Second, burrowing animals affect early diagenesis by ventilating the seafloor and shallow pore fluids (Aller, 1994). Reactions with oxygen, especially aerobic respiration and sulfide oxidation, produce dissolved inorganic carbon (DIC) and/or consume alkalinity in ratios that are below 1:1, which are unfavorable for carbonate cementation and preservation (Bergmann et al., 2013; Higgins et al., 2009; Knoll et al., 2011; Walter & Burton, 1990). By this mechanism, animals may suppress flat pebbles by supplying oxygen to the taphonomically active zone beneath the sediment-water interface (Wright & Cherns, 2016).

Unravelling the mechanisms by which animal behaviors suppress flat pebbles is critical for interpreting these textures in the geologic record. If an oxygen-poor environment is needed, then flat pebbles imply local anoxia near the sediment-water interface (Wignall & Twitchett, 1999) and therefore may mark low shallow-marine oxygen levels or high organic matter fluxes within Cambro-Ordovician (Saltzman et al., 2015) and Early Triassic shelves (Wignall & Twitchett, 1999). If instead animals reduce sediment cohesion by physically disrupting sediments, then cohesion might scale inversely with body size, population density, and ecospace use (Bush et al., 2007; Droser et al., 1997). Substrate changes would signal changes in animal density or behavior without implying specific environmental conditions such as anoxia. Thus, understanding how flat-pebbles form would tell us if they are markers for changes in carbonate chemistry, animal behavior, or both across Earth history.

The rarity of flat-pebble conglomerates in modern carbonate-forming environments presents a significant challenge to understanding the processes and conditions of flat-pebble formation. Here we present results from a study of a modern process analog for these facies in the Great Salt Lake of Utah, in the Western US. The objectives of this work were to (1) document facies patterns, mineralogy, and cement morphologies within clasts; (2) determine how frequently sediment comprising flat pebbles is transported near the field site; (3) compare the chemical and physical work done on sediments in the Great Salt Lake to those in modern marine carbonate-producing environments to better understand how cohesive substrates form; and (4) use this insight to update possible interpretations of substrate changes associated with Phanerozoic radiations and extinctions.

2 Geologic Setting and Ecology of Great Salt Lake

The Great Salt Lake (northwestern Utah, USA) is a remnant of a larger, deeper lake system in the Great Basin (Gilbert, 1890). Its immediate precursor, Lake Bonneville, formed at *ca*. 30 ka and was characterized by higher and more variable lake levels (Oviatt et al., 1992).

Bonneville shorelines preserve carbonate facies characteristic of freshwater and saline or alkaline lakewater mixing zones, such as tufas and microbialites (Felton et al., 2006; Nelson et al., 2005). The basinward extent of these shoreline facies was limited by steep margins and high-amplitude lake fluctuations (Vennin et al., 2019). The transition to the modern Great Salt Lake occurred during mid-Holocene time (~11.5 ka), resulting in lower lake levels, higher salinities, and smaller amplitude fluctuations in lake volume (Oviatt et al., 1992). This transition also coincided with an increase in carbonate sediments as recorded in cores (Thompson et al., 1990). Although lake volume has remained relatively stable since 9,000 y B.P., lake chemistry has continued to evolve through changing hydrology and the precipitation of halite along with minor sulfate salts (Jones et al., 2009). Modern lake chemistry also reflects anthropogenic changes, most notably a causeway built in 1959 that divides the lake into northern and southern 'arms' (Spencer et al., 1985). The Bear, Weber, and Jordan Rivers provide freshwater inputs to the South Arm, but the North Arm is hydrologically closed and, therefore, only recharged by local precipitation. The hydrological restriction of the North Arm resulted in salinities ranging from 24 to 31% compared to 11 to 14% in the South Arm (Cannon & Cannon, 2002). Both sub-basins are at least three times more saline than seawater. Average dissolved oxygen levels in GSL surface waters ranged from 6.46-8.71 mg/L in 2011-2012 (Utah Department of Water Quality, 2014), although the deep brine layer that occurs below 6.3 m water depth is anoxic (Wurtsbaugh and Jones, 2012). Assays for porewater sulfide in GSL indicated that shallow porewaters (<12 cm below the sediment-water interface) in ooid sand facies are typically oxic (Ingalls et al., 2020).

In salt lakes, species diversity and richness are inversely correlated with salinity (Williams et al., 1990). Food webs in Great Salt Lake are phytoplankton-based, with invertebrate ecology dominated by a few abundant, salt-tolerant taxa (i.e., brine shrimp [*Artemia*], brine flies [*Ephydridae*], and corixids; Belovsky, 2011). The highly restricted taxonomic diversity, community structure, and small size of these metazoans limits animal-sediment interactions in these systems, even though biomass can be locally high. *Artemia* are the most abundant macro-organisms in GSL, and they feed on phytoplankton in the water column (Belovsky et al., 2011; Wurtsbaugh, 1992). In contrast, brine flies, which contribute ~70% less biomass than brine shrimp to the GSL ecosystem, feed on benthic substrates, including microbial mat communities associated with microbialites (Collins, 1980; Wurtsbaugh, 2009). However, none of the documented taxa in the lake build habitation burrows below the sediment-water interface; there is also no deposit-feeding.

The study area was along the southwest coastline of Antelope Island, South Arm, near the Miera Spit (Fig. 1). Nearshore sediments are composed of ooid sands and unusual deposits of thin, pebble-sized clasts. Eardley (1938) termed these 'hydrogenic shingles' as they are composed of cemented ooids rather than detrital clasts of nearby bedrock. These 'hydrogenic shingles' have received little attention in the literature compared to GSL microbialites, which have been studied in terms of their facies distribution (Bouton, Vennin, Boulle, et al., 2016; Bouton, Vennin, Mulder, et al., 2016), petrography (Vennin et al., 2019), mineralogy, and biogeochemistry (Pace et al., 2016). Efforts to understand biological mediation of carbonate chemistry in GSL have been aided by ongoing studies of microbial communities and biogeochemistry, both in surface water and near-surface porewaters (Dunham et al., 2020; Ingalls et al., 2020). The thin, platy shingles associated with wave-dominated shorelines strikingly resemble intraclasts commonly found in Paleozoic marine environments (e.g. Myrow et al., 2004), motivating detailed study of the aforementioned process sedimentology, biogeochemistry, diagenesis, and facies of flat-pebble deposits in Great Salt Lake.

3 Methods and Data

3.1 Sample Collection and Analysis

Field data and samples were collected in September 2019. Grain size distributions for unconsolidated sediments were measured using a Retsch Camsizer P4 at the University of Colorado Boulder. Representative hand samples of flat pebbles were cut into thin sections and impregnated with either clear or blue epoxy. Microscale chemical imaging of thin sections was performed at the California Institute of Technology using a Bruker M4 Tornado μXRF-EDS run at 50 keV with a 10 ms dwell time on 20 μm pixels. Facies maps were constructed using field mapping, geotagged images, and satellite data accessed through Google Earth™ (images: Landsat/Copernicus). Additional constraints on lake history within the field site were provided by satellite imagery (2007-2019) and historical lake levels available through the US Geological Survey (1847-2019, https://nwis.waterdata.usgs.gov/).

3.2 Linear Wave Models for Sediment Transport

Many ancient flat-pebble facies formed by storm-reworking of early cemented crusts (e.g., Lee & Kim, 1992; Markello & Read, 1981; Myrow et al., 2004; Sepkoski, 1982). Such deposits imply that high-energy storm events are separated by periods of relative quiescence during which early cements take hold in pore spaces. To investigate the potential role of wave energy, we estimated historical conditions using a linear wave model based on wind data from the University of Utah's Mesowest database (Horel et al., 2002). Wind data were selected from a station on Hat Island, covering 7,255 days from 1998-2020 (Fig. 2a). Data were averaged over 4-hour intervals using the openair package in R (Carslaw & Ropkins, 2012) to resolve features such as squalls and diurnal variations in wind speed and direction.

Wave models were constructed using a python-based toolbox for arcMap (J. Rohweder et al., 2012; J. J. Rohweder et al., 2008). Lake bathymetry and shoreline position were calculated from the digital elevation model (DEM) of Tarboton (2017) using an average lake level of 1279.15 m from 1997-2018 as calculated from USGS measurements (Fig. 2b). Eighteen fetch maps were constructed in 20° segments, and maps were produced for wave heights, period, and shear velocities for wind speeds ranging from 10-90 mph (Fig. 2c, d). The resulting map of shear velocities was examined at two points off the west coast of Antelope Island: the western edge of the bedforms visible in satellite data (points A and B in Fig. 1c).

4 Results

4.1 Petrography and Sample Description

Beach sediments consisted of medium to coarse sand-sized peloids, ooids, grapestones, and minor lithic fragments intermixed with pebble- to cobble-sized ooid grainstone intraclasts. Two representative ooid sand samples, GSL19-2 and GSL19-5, have median grain diameters (D_{50}) of 665 and 648 μm, respectively (Fig. 4d). The intraclasts have diameters ranging from <1 to 20 cm, subangular to subrounded edges, and a near-uniform thickness of ~1 cm. Transmitted light microscopy of thin sections from cemented clasts revealed that ooids are coated with isopachous rinds of inclusion-poor cement crystals (Fig. 3a). Towards the center of the clasts, isopachous cements are composed of small (~5 μm), equant to anhedral to subhedral crystals (Fig. 3d). Cements are better developed near clast edges, and in some cases occluded most of the intergranular pore space. Cement crystals near the clast edges are also larger (10-30 μm lengthwise) and displayed bladed morphologies with flat-tipped terminations (Fig. 3c). The flat-tipped crystal habits are consistent with aragonite cements documented from modern and ancient (Loucks & Folk, 1976) marine and/or evaporitic environments. Near clast edges, these clear isopachous cements overgrew an earlier dark,

cryptocrystalline cement that created concave bridges between some grains and sometimes displayed faint laminations (Fig. 3e). However, the cryptocrystalline cements are relatively rare compared to the clear isopachous cements which are found everywhere.

4.2 Satellite Imagery and Field Mapping

Satellite images and field mapping reveals two large-scale features associated with flat-pebble deposits. The first is a patch of NNW-SSE trending, low sinuosity bedforms that extends for 200 m south of the Miera Spit (Fig. 4). The bedforms have a median crestline length of 40 m (range 10-169 m), with larger straight-crested bedforms nearest the spit, and smaller barchanoid shapes further south. Both satellite imagery (Fig. 4b,c) and lake level data from the USGS show that these previously submerged features were exposed as lake levels fell ~1.2 m from 2011 to 2019 (1279.3 m to 1278.1 m). The second feature is a low-relief ridge developed along the present-day shoreline. The ridge, which is visible in imagery from 2015 onwards (Fig. 4c), is discontinuous along strike and displays cuspate morphologies.

Sedimentary structures in both unconsolidated ooids and intraclasts change with distance from the shoreline. Intraclasts are nearly absent far behind the swash zone, and beach sediments are characterized by lithic-rich ooid sand with rare, discontinuous meter-scale patches of wind rippled sand (Fig 5a). Rippled sediments are coarser (including ooids with diameters >1 mm) than the surrounding deposits. Far from the shoreline, intraclasts are smaller (1-2 cm in diameter) and are arranged into flat pavements (Fig. 5b). Clast size and frequency increase closer to the shoreline (Fig. 5c), with the higher clast abundances atop topographic highs; this includes both the low-sinuosity bedforms near the spit and the shoreline-parallel ridge behind the swash zone (Fig 5e). Intraclasts are locally imbricated and arranged into rosettes, (Fig. 5d), which are common bedforms produced by wave reworking of clasts with low advection length-scale transport in gravel-rich beach and shoreface settings (Sanderson & Donovan, 1974).

Two complementary observations indicated that the clasts were formed by erosion and re-deposition of early-cemented subaqueous crusts/hardgrounds. As noted above, the frequency and size of clasts decrease away from the shoreline, implying that older clasts were either abraded or buried by sand-sized particles as they were transported up the beach. A more robust constraint on the source of large clasts is the ubiquitous presence of lithified symmetrical (and trochoidal) wave-ripples (Fig. 5f), with the best-preserved bedforms found near the present-day shoreline. The preserved wave ripples offer an important time constraint as they must have lithified more quickly than they could be reworked by aeolian processes during exposure.

Both aerial imagery and historical lake records indicate that some features observed are relict deposits from intervals of higher lake levels, rather than a depositional profile that is in equilibrium with the current shoreline. We therefore constructed an idealized depositional profile for a period of stable base level (Fig. 5g). The supratidal environments landward of the shoreline were grainy deflation flats with few sedimentary structures other than starved wind- and wave-ripples. Intraclast content increases downdip towards the beach, with higher abundances concentrated in the foreshore and storm-berm environments. The upper shoreface consists of symmetrical, sharp-crested wave ripples and larger bar forms that were ultimately the source of early cemented material for intraclasts.

4.3 Elemental Mapping

The relative elemental abundances informed phase identification and trace element compositions of the ooid grains (nuclei and cortices) and cements (Fig. 6) that comprised representative clasts. Lithic fragments and some ooid nuclei are rich in silicon, potassium,

and iron associated with siliciclastic minerals identified in hand specimens such as quartz, feldspars, and hornblende—phases derived from the upland bedrock exposed on Antelope Island. Ooid cortices and cements are rich in calcium, with secondary peaks in magnesium and strontium, both of which are commonly incorporated into aragonite and high-magnesium calcite. The compositional data and the observed crystal morphologies suggest that aragonite is the primary carbonate phase in the grains and cements, though we cannot rule out the presence of minor/trace phases such as dolomite, magnesite, and Mg-silicates intergrown at the micron scale—each of these phases have been reported from Great Salt Lake and Lake Bonneville sediments (Dunham et al., 2020; Graf et al., 1961; Pace et al., 2016) Additional maps of S, Na, and Cl revealed that grains are not cemented by evaporite minerals such as gypsum ($CaSO_4{\cdot}2H_2O$), halite (NaCl), or mirabolite ($Na_2SO_4{\cdot}10H_2O$) (Jones et al., 2009).

4.4 Comparing Timescales of Cement Growth and Sediment Transport

To untangle potential physical and chemical processes that might impact cementation near the sediment-water interface—and by extension, the production of flat pebbles—we developed simple frameworks that weigh the chemical drivers for cement growth against physical energy from waves and bioturbating organisms.

The first approach compares the timescales associated with cement growth against the frequency with which grains are suspended near Antelope Island. Experiments have demonstrated that precipitation (or dissolution) rates for carbonate minerals scale with the $CaCO_3$ saturation state (Ω) via the following expression (Zhong & Mucci, 1989):

$$R = k(\Omega - 1)^n \quad \text{(Eqn. 1)}$$

where R is the precipitation rate in moles per unit area, n is the reaction order (typically empirically determined), and k is an empirical rate constant ($\mu mol\, m^{-2}\, h^{-1}$). The saturation state of a fluid with respect to aragonite is a measure of the thermodynamic drive for aragonite precipitation, expressed as Ω_{arag}— a measure of the deviation of the ion activity product of Ca^{2+} and CO_3^{2-} from the thermodynamic solubility product of aragonite ($\{Ca^{2+}\}\{CO_3^{2-}\}/K_{sp}$). If the relevant constants and range of saturation states are known, the timescale growing cement crystals of a particular length, Δx, can be estimated as:

$$\Delta t = \frac{\rho_{arag}\Delta x}{M_{arag}k(\Omega - 1)^n} \quad \text{(Eqn. 2)}$$

Where ρ_{arag} and M_{arag} are the density and molar mass of aragonite, respectively. The timescales associated with precipitation of ~5-μm-thick cements, such as those in Figure 3d, were between 38 and 460 days using Ω_{arag} values of 2-4 reported by Ingalls et al. (2020) and the values for constants in Table 1.

The seemingly delicate cements indicate intervals of minimal sediment transport that allowed cement growth to bind intraclasts before erosion, entrainment, and re-deposition. The timescales associated with sediment transport were estimated from wave models and compared to the cement timescales derived above. Wind events from 1998-2020 were classified according to shear velocity maps with a cutoff of 8 cm/s—the value necessary for transport at the threshold of suspension for ~650 μm particles in the southern Arm of GSL. This critical bed shear velocity was calculated using the Rouse number, $P = \frac{w_s}{\kappa u_*}$, where P = 2.5 corresponds to transport at the threshold of suspension, w_s is settling velocity calculated following Dietrich (1982), κ=0.41 is the dimensionless von Kárman constant, and u_* is bed shear velocity. The distribution of non-consecutive transport events near the field site (points A and B in Fig. 1c) had an average of 20-21 days. Importantly, the longest duration between events—187 days between March and September in 2014—sat within the range of cement

timescales calculated above (Fig. 7). Once adjacent particles become cemented together into compound particles, the larger effective diameter of the compound particles would increase the thresholds for motion and suspension, decreasing the frequency of transport further. Interestingly, the timescales calculated above are all subannual; at longer timescales, the interplay between changes in Ω (via changes in river discharge) and regional wind patterns could play an additional role in cementation. Nevertheless, these simplified calculations suggest that a near-parity between the timescales of cementation and transport is a minimum prerequitiste for intraclast formation.

4.5 Transfer of physical energy through bioturbation

During extended hiatuses in sediment transport, bioturbating organisms supply additional kinetic energy to the substrate, engendering a second competition between precipitation and cement disruption. As cements grow, the change in surface area of the aragonite-water phase boundary within pores carries with it an associated energy change (Berner, 1980):

$$dE = \sigma \cdot dA \quad \text{(Eqn. 3)}$$

where *dE* is energy change [J], σ is the interfacial free energy between aragonite and water [J m^{-2}], and *dA* [m^2] denotes changes in surface area. Cement growth into open pores reduces the available surface area, resulting in a reduction in interfacial free energy (Fig. 8a-c). Using a simple relationship between porosity and surface area given by Emmanuel & Berkowitz (2005), the instantaneous rate of change for surface energy can be approximated as:

$$\frac{dE}{dt} \approx -\sigma \frac{2}{3} \frac{(A_i)^2}{V_t} \frac{k\left(\Omega_{arag} - 1\right)^n}{\rho_{arag}} M_{arag} \quad \text{(Eqn. 4)}$$

where A_i is the initial surface area, V_t is the total volume (minerals + pore water) of interest [see SI 1]. Values for these parameters in the literature are given in Table 1. Eqn. 4 primarily depends on porosity, initial surface area (a combination of grain size and roughness), and the aragonite saturation state. For direct comparison, we assumed equivalent surface area and porosity relations between marine ooids and those in Great Salt Lake, and only considered differences in aragonite saturation (Rankey & Reeder, 2009; Trower et al., 2017).

In contrast, burrowing organisms increase the surface area of cements by crushing or grinding incipient cements (Fig. 8). Burrowing organisms lose some of their energy as external work on sediments, much of which results in inelastic deformation (Dorgan et al., 2011). One can interpret this external work as energy available to increase surface area, yielding:

$$\frac{dE_{burrow}}{dt} = C \cdot v \cdot B \quad \text{(Eqn. 5)}$$

where *C* is an energetic cost per unit biomass (Dorgan et al., 2011), *v* is the velocity at which organisms burrow (Gingras et al., 2008), and *B* is the total infaunal biomass within a given sediment volume of interest. For this analysis, we assumed that the infaunal biomass density, B, was the main variable governing energy transfer across the sediment-water interface.

Changes in interfacial energy due to growth and breakage have opposing effects on sediment cohesion; cement growth will bind particles while bioturbation will loosen them. The combined effects of cementation and burrowing were scaled by comparing the relative contributions of growth and breakage to total surface energy (Fig. 8d). This framework also permitted comparison between GSL and marine systems. For example, in the Great Barrier Reef (Alongi, 1989), the relative change in energy due to bioturbation varied over more than two orders of magnitude, from less than 1:1 to greater than 100:1 depending on the biomass

density and the linear burrowing rate of infaunal taxa. We also plotted environments from the Persian Gulf that have benthic biomass densities that are comparable to the Great Barrier Reef (Coles & McCain, 1990) but have higher ambient aragonite saturation states (Rivers et al., 2019). Great Salt Lake, however, lacks the infaunal communities present in marine settings and thus has no meanginful energy transfer due to bioturbation.

This comparison between marine systems and Great Salt Lake relied on a few assumptions. First, the rate law in Eqn. 1 assumes that empirically determined constants for the rate law are similar for both seawater and GSL water. While GSL water is three times more saline than seawater, the constants under these conditions have not been experimentally determined. Another possibility is that cohesion contains components from additional, non-carbonate authigenic phases that are below the spatial resolution of the µXRF (~20 µm) and the light microscopy (~1 um). In particular, Mg-Si clays have been documented in Great Salt Lake within both surface microbial mats (Pace et al., 2016) and within shallow sediments (Ingalls et al., 2020). However, our petrographic and chemical imaging indicated that aragonite cements are predominant binders in these clasts (Fig. 3, Fig. 6), and any additional phases would share the same physical environmental constraints.

5 Discussion

5.1 Depositional Setting of Flat Pebbles in Great Salt Lake

Early lithified substrates in Great Salt Lake differed from those commonly found in modern marine settings. For example, in open marine settings, carbonate cements often precipitate in the swash zone, producing a texture known as beachrock (Vousdoukas et al., 2007). Once formed, beachrock can be redeposited offshore during storms as clasts in a grainstone matrix (Kerans et al., 2019). Clasts can also form in the intertidal and supratidal zones through the breakdown of lithified mats (Shinn, 1983) and tepee structures (Lokier & Steuber, 2009). The aforementioned cases all share an offshore-directed sense of transport with the majority of cements forming near or landward of the shoreline. In contrast, observations from Great Salt Lake showed that clasts formed offshore and were transported landward. The cements are isopachous (Fig. 3b-d)—a texture that typically forms in phreatic environments—and lack vadose textures such as dripstone or meniscus cements (James & Choquette, 1984). The presence of lithified trochoidal wave ripples (Fig. 5f) provided further evidence that the clasts formed from subaqueous crusts near the sediment-water interface. The landward decrease in clast size and abundance (Fig. 5b-c) indicate clast breakdown during onshore-directed transport. Overall, the style of early diagenesis in Great Salt Lake better matches widespread subaqueous crusts documented from the Persian Gulf (Shinn, 1969) than those that form in open marine settings.

Flat-pebble facies in Great Salt Lake shared important parallels with ancient marine deposits. Many ancient examples of intraclast conglomerates are interpreted as storm deposits associated with wave-dominated environments (Lee & Kim, 1992; Markello & Read, 1981; Myrow et al., 2004; Sepkoski, 1982). While bathymetries and wave parameters may differ between GSL and marine settings, the lake nonetheless provides a process analog in terms of the frequency of sediment transport. Myrow et al. (2004) categorized flat-pebble conglomerates according to their depositional environments, which included documented occurrences of beach deposits. Beaches consisted of shallowing-upwards packages of hummocky grainstones capped by flat pebbles with wave-reworked “rosettes” (their Fig. 12). The general pattern observed by Myrow et al., (2004)—wave-dominated bedforms (hummocks or ripples) passing into flat-pebble beaches—suggested a depositional model similar to the facies arrangement in Fig. 5g. While this study focused on intraclast

conglomerate development in nearshore environments, it is likely that there are also examples of offshore-directed transport deeper in the lake. Overall, Great Salt Lake is a useful analog for understanding chemical and biological controls on flat-pebble formation, even for strata that accumulated under different depositional environments earlier in Earth history.

5.2 Biological, Physical, and Chemical controls on flat pebble deposits

One hypothesis we sought to test was whether or not flat pebbles in GSL could be explained by chemical drivers attributable to lakewater carbonate chemistry (i.e. flat pebbles tied to anomalously high aragonite saturation states). However, comparisons among GSL and marine settings preclude this explanation (Fig. 8d). Ingalls et al. (2020) found saturation states near $\Omega_{aragonite}$=2 from samples of surface water and shallow pore waters in GSL. Although values indicated that aragonite should precipitate in these environments—consistent with our petrographic observations—these values are lower than typical saturation states for tropical surface seawater ($\Omega_{aragonite}$=3-5) (Jiang et al., 2015; Trower et al., 2018) and much lower than those in the Persian Gulf where saturation states may reach as high as $\Omega_{aragonite}$=10 in coastal embayments (Rivers et al., 2019). Assuming parameters from Zhong & Mucci (1989) (Table 1) also hold for GSL salinity, then kinetic growth rates for carbonate minerals should actually be substantially slower in GSL than in marine settings. An alternate explanation, then, is that slow reaction kinetics are offset by a lack of physical energy supplied to the sediment-water interface.

While it is unsurprising that infrequent transport favors early cements, our observations from Great Salt Lake highlight the importance of bioturbation in providing an alternative source of kinetic energy in such environments. The idea that organisms physically alter sediments probably originated with Darwin's studies of earthworms (Darwin 1881), yet it has found increasing applications in terrestrial landscape evolution (Phillips, 2009). For example, Yoo et al. (2005) showed that gopher burrows are major contributors to hillslope creep, even though gophers expend <0.001% of the ecosystem's energy budget to move sediment. This body of work has demonstrated how even a tiny fraction of the energy transduced through ecosystems—when integrated over time—can accomplish substantial work in terms of sediment mass flux. The results presented here from Great Salt Lake suggested to us that similar arguments could be applied to the development of lithified substrates in subaqueous systems. The difference in animal biomass—and by extension, the physical energy transferred to sediments during burrowing—best explains why flat pebbles form in Great Salt Lake, even though modern marine settings have higher $\Omega_{aragonite}$ values. Additionally, the diverse, abundant, and stable microbial communities in GSL can be viewed as a side-effect of low burrowing animal abundances on the lake floor. If biofilms are physical and/or chemical contributors to stable substrates, then animals exert an indirect control by grazing them.

5.3 Implications for Ancient Flat-pebble Deposits

As a process analog, Great Salt Lake emphasized the role of physical energy, introduced by animal behaviors such as feeding and burrowing, in determining substrate cohesion. In contrast, pebbles in Great Salt Lake formed in ooid sands that are not strongly anoxic near the sediment-water interface (<12 cm) or within the water column (Wurtsbaugh and Jones, 2012; Utah Department of Water Quality, 2014; Ingalls et al., 2020). The latter finding is particularly significant as ancient flat pebbles are often interpreted as evidence for enhanced carbonate precipitation under anaerobic conditions (Wignall & Twitchett, 1999; Wright & Cherns, 2016). The dependency of substrate cohesion on physical factors such as total infaunal density (Fig. 7e) and ecological tiering makes it difficult to untangle potential relationships between flat-pebbles and redox. Instead, the disappearance of these facies could

be explained by an increase in total infaunal biomass driven by increasing growth and consumption efficiency (Payne & Finnegan, 2006), which would explain any discrepancies between flat pebbles and geochemical redox proxies. Perhaps the Early Paleozoic platforms were similar to Great Salt Lake in that they were characterized by well-oxygenated seawater that was moderately supersaturated with respect to $CaCO_3$, but much lower infaunal densities than modern marine environments.

Flat-pebble facies are also well-known from Early Triassic deposits in China, Italy, and the western US (Pruss et al., 2005; Wignall & Twitchett, 1999). The Early Triassic represents a prolonged recovery after the end-Permian extinction, and flat-pebbles are consistent with other evidence for low infaunal biomass such as small body sizes (Payne & Finnegan, 2006; Payne et al., 2006) and reduced size and tiering among trace fossils (Pruss & Bottjer, 2004; Twitchett, 1999). Putative mechanisms of delayed recovery include anoxia (Lau et al., 2016), hypercapnia (high pCO_2) (Knoll et al., 2007), saturation state crises (Knoll and Fischer 2011), high thermal stresses (Sun et al., 2012), and reduced competition among species (Hautmann et al., 2015). These results from Great Salt Lake suggest that flat pebbles are consistent with any of these causes. The analysis captured in Fig. 8d indicates that reduced biomass density—perhaps several orders of magnitude (Payne & Finnegan, 2006)—would have itself led to more lithified substrates. Under this interpretation, flat pebbles would provide a measure of how severe an extinction is, rather than serve as an indicator of extinction mechanisms.

Finally, early cemented substrates from Great Salt Lake may have significance beyond Phanerozoic deposits. Stromatolites, carbonate fans, and other Precambrian facies often are taken as evidence that the $CaCO_3$ saturation state of the ocean has generally declined from the late Archean to present (Bergmann et al., 2013; Cantine et al., 2020; Grotzinger & James, 2000). Yet, an emerging view is that the $CaCO_3$ saturation state in early anoxic oceans was perhaps even lower than in marine basins today (Blättler et al., 2017; Higgins et al., 2009). The results of this study indicates that the absence of animal-sediment interactions permits near-surface cementation under a wide range of saturation states.

6 Conclusions

The existence of flat pebble conglomerates in Great Salt Lake provides a useful process analog for Early Paleozoic marine environments, when substrate cohesion was greater than in marine shelf environments today. The style of early lithification documented here is distinct from other shoreline facies, such as beachrock. Aragonite saturations are surprisingly low both within porewaters and surface water, which remain largely oxygenated (Ingalls et al., 2020), such that the presence of flat-pebble facies here cannot be explained by mechanisms that invoke high $CaCO_3$ saturation states and/or anoxia. Instead, intermittent sediment transport and an absence of burrowing organisms in Great Salt Lake permits high sediment cohesion induced by the growth of aragonite cements. By analogy, ancient flat-pebble conglomerates could simply represent periods of low animal biomass in storm-dominated shelves, by limiting the transfer of physical energy across the sediment-water interface. Together our observations and analyses suggested that the physical work done by burrowing animals to break up nascent cements in surface sediment is equally or more important than potential chemical drivers typically allied with redox processes and marine carbonate chemistry. Finally, flat pebbles in Great Salt Lake served as a reminder that while metazoan life plays an important chemical and ecological roles in carbonate environments (e.g. the production of sediment via carbon skeletons), it also plays an critical role in sediment transport. Interpretations of long-term changes in the prevalence of carbonate facies such as

stromatolites, crystal fans, and flat pebbles in the rock record could profitably consider physical energy budgets in tandem with the chemical evolution of Earth's oceans.

Acknowledgments, Samples, and Data

B. Smith acknowledges support from the Agouron Institute Postdoctoral Fellowship and thanks Christine Chen and John Grotzinger for insightful feedback on this project. W. Fischer acknowledges support from the American Chemical Society Petroleum Research Fund, Caltech's Rothberg Innovative Initiative, and the Caltech Center for Evolutionary Science. This study was made possible in part due to the data made available by the governmental agencies, commercial firms, and educational institutions participating in MesoWest. The authors are not aware of any conflicts of interest.

The codes for this project are hosted on Github (http://doi.org/10.5281/zenodo.3873704). Wind data are available through https://mesowest.utah.edu/. Sample information can be accessed through the System for Earth Sample Registration SESAR using the tags IEBPS0001-0002 for intraclasts and IEEJT004U and IEEJT004UX for unconsolidated ooids. Historical lake level data can be acquired from the USGS (https://nwis.waterdata.usgs.gov/).

References

Aller, R. C. (1994). Bioturbation and remineralization of sedimentary organic matter: effects of redox oscillation. Chemical Geology, 114(3–4), 331–345.

Alongi, D. M. (1989). Benthic processes across mixed terrigenous-carbonate sedimentary facies on the central Great Barrier Reef continental shelf. Continental Shelf Research, 9(7), 629–663. https://doi.org/10.1016/0278-4343(89)90034-4

Belovsky, G. E., Stephens, D., Perschon, C., Birdsey, P., Paul, D., Naftz, D., et al. (2011). The Great Salt Lake Ecosystem (Utah, USA): long term data and a structural equation approach. Ecosphere, 2(3), art33. https://doi.org/10.1890/ES10-00091.1

Bergmann, K. D., Grotzinger, J. P., & Fischer, W. W. (2013). Biological influences on seafloor carbonate precipitation. Palaios, 28(2), 99–115.

Berner, R. A. (1980). Early diagenesis: a theoretical approach. Princeton University Press.

Blättler, C. L., Kump, L. R., Fischer, W. W., Paris, G., Kasbohm, J. J., & Higgins, J. A. (2017). Constraints on ocean carbonate chemistry and p CO 2 in the Archaean and Palaeoproterozoic. Nature Geoscience, 10(1), 41.

Bouton, A., Vennin, E., Mulder, T., Pace, A., Bourillot, R., Thomazo, C., et al. (2016). Enhanced development of lacustrine microbialites on gravity flow deposits, Great Salt Lake, Utah, USA. Sedimentary Geology, 341, 1–12.

Bouton, A., Vennin, E., Boulle, J., Pace, A., Bourillot, R., Thomazo, C., et al. (2016). Linking the distribution of microbial deposits from the Great Salt Lake (Utah, USA) to tectonic and climatic processes. Biogeosciences, 13(19).

Bush, A. M., Bambach, R. K., & Daley, G. M. (2007). Changes in theoretical ecospace utilization in marine fossil assemblages between the mid-Paleozoic and late Cenozoic. Paleobiology, 33(1), 76–97.

Cannon, J. S., & Cannon, M. A. (2002). The Southern Pacific Railroad trestle—past and present. Great Salt Lake, an Overview of Change, 283, 294.

Cantine, M. D., Knoll, A. H., & Bergmann, K. D. (2020). Carbonates before skeletons: A database approach. Earth-Science Reviews, 201, 103065. https://doi.org/10.1016/j.earscirev.2019.103065

Carslaw, D. C., & Ropkins, K. (2012). Openair—an R package for air quality data analysis. Environmental Modelling & Software, 27, 52–61.

Coles, S. L., & McCain, J. C. (1990). Environmental factors affecting benthic infaunal communities of the Western Arabian gulf. Marine Environmental Research, 29(4), 289–315. https://doi.org/10.1016/0141-1136(90)90024-I

Collins, N. (1980). Population ecology of Ephydra cinerea Jones (Diptera: Ephydridae), the only benthic metazoan of the Great Salt Lake, USA. Hydrobiologia, 68(2), 99–112.

Darwin, C. (1881). The formation of vegetable mould through the action of worms: with observations on their habits (Vol. 37). Appleton.

Dietrich, W. E. (1982). Settling velocity of natural particles. Water Resources Research, 18(6), 1615–1626.

Dorgan, K. M., Lefebvre, S., Stillman, J. H., & Koehl, M. A. R. (2011). Energetics of burrowing by the cirratulid polychaete Cirriformia moorei. Journal of Experimental Biology, 214(13), 2202–2214.

Droser, M. L., & Bottjer, D. J. (1989). Ordovician increase in extent and depth of bioturbation: Implications for understanding early Paleozoic ecospace utilization. Geology, 17(9), 850–852.

Droser, M. L., Bottjer, D. J., & Sheehan, P. M. (1997). Evaluating the ecological architecture of major events in the Phanerozoic history of marine invertebrate life. Geology, 25(2), 167–170.

Dunham, E. C., Fones, E. M., Fang, Y., Lindsay, M. R., Steuer, C., Fox, N., et al. (2020). An Ecological Perspective on Dolomite Formation in Great Salt Lake, Utah. FrEaS, 8, 24.

Eardley, A. J. (1938). Sediments of Great Salt Lake, Utah. AAPG Bulletin, 22(10), 1305–1411.

Emmanuel, S., & Berkowitz, B. (2005). Mixing-induced precipitation and porosity evolution in porous media. Advances in Water Resources, 28(4), 337–344.

Felton, A., Jewell, P. W., Chan, M., & Currey, D. (2006). Controls of tufa development in pleistocene lake Bonneville, Utah. The Journal of Geology, 114(3), 377–389.

Gilbert, G. K. (1890). Lake Bonneville (Vol. 1). US government printing office.

Gingras, M. K., Pemberton, S. G., Dashtgard, S., & Dafoe, L. (2008). How fast do marine invertebrates burrow? Palaeogeography, Palaeoclimatology, Palaeoecology, 270(3–4), 280–286.

Graf, D. L., Eardley, A. J., & Shimp, N. F. (1961). A preliminary report on magnesium carbonate formation in glacial Lake Bonneville. The Journal of Geology, 69(2), 219–223.

Grotzinger, J. P., & James, N. P. (2000). Precambrian carbonates: evolution of understanding.

Hautmann, M., Bagherpour, B., Brosse, M., Frisk, Å., Hofmann, R., Baud, A., et al. (2015). Competition in slow motion: the unusual case of benthic marine communities in the wake of the end-Permian mass extinction. Palaeontology, 58(5), 871–901. https://doi.org/10.1111/pala.12186

Higgins, J. A., Fischer, W. W., & Schrag, D. P. (2009). Oxygenation of the ocean and sediments: consequences for the seafloor carbonate factory. Earth and Planetary Science Letters, 284(1–2), 25–33.

Horel, J., Splitt, M., Dunn, L., Pechmann, J., White, B., Ciliberti, C., et al. (2002). Mesowest: Cooperative mesonets in the western United States. Bulletin of the American Meteorological Society, 83(2), 211–226.

Ingalls, M., Frantz, C. M., Snell, K. E., & Trower, E. J. (2020). Carbonate facies-specific stable isotope data record climate, hydrology, and microbial communities in Great Salt Lake, UT. Geobiology, n/a(n/a). https://doi.org/10.1111/gbi.12386

James, N. P., & Choquette, P. W. (1984). Diagenesis 9. Limestones-the meteoric diagenetic environment. Geoscience Canada, 11(4).

Jiang, L.-Q., Feely, R. A., Carter, B. R., Greeley, D. J., Gledhill, D. K., & Arzayus, K. M. (2015). Climatological distribution of aragonite saturation state in the global oceans. Global Biogeochemical Cycles, 29(10), 1656–1673.

Jones, B. F., Naftz, D. L., Spencer, R. J., & Oviatt, C. G. (2009). Geochemical evolution of great salt lake, Utah, USA. Aquatic Geochemistry, 15(1–2), 95–121.

Kerans, C., Zahm, C., Bachtel, S. L., Hearty, P., & Cheng, H. (2019). Anatomy of a late Quaternary carbonate island: Constraints on timing and magnitude of sea-level fluctuations, West Caicos, Turks and Caicos Islands, BWI. Quaternary Science Reviews, 205, 193–223.

Knoll, A. H., Bambach, R. K., Payne, J. L., Pruss, S., & Fischer, W. W. (2007). Paleophysiology and end-Permian mass extinction. Earth and Planetary Science Letters, 256(3), 295–313. https://doi.org/10.1016/j.epsl.2007.02.018

Knoll, A. H., Fischer, W. W., Gattuso, J. P., & Hansson, L. (2011). Skeletons and ocean chemistry: the long view. Ocean Acidification, 4, 67-82.

Lau, K. V., Maher, K., Altiner, D., Kelley, B. M., Kump, L. R., Lehrmann, D. J., et al. (2016). Marine anoxia and delayed Earth system recovery after the end-Permian extinction. Proceedings of the National Academy of Sciences, 113(9), 2360–2365.

Lee, Y. I., & Kim, J. C. (1992). Storm-influenced siliciclastic and carbonate ramp deposits, the Lower Ordovician Dumugol Formation, South Korea. Sedimentology, 39(6), 951–969.

Lokier, S., & Steuber, T. (2009). Large-scale intertidal polygonal features of the Abu Dhabi coastline. Sedimentology, 56(3), 609–621.

Loucks, R. G., & Folk, R. L. (1976). Fanlike rays of former aragonite in Permian Capitan Reef pisolite. Journal of Sedimentary Research, 46(3), 483–485.

Markello, J. R., & Read, J. F. (1981). Carbonate ramp-to-deeper shale shelf transitions of an Upper Cambrian intrashelf basin, Nolichucky Formation, Southwest Virginia Appalachians. Sedimentology, 28(4), 573–597.

Myrow, P. M., Tice, L., Archuleta, B., Clark, B., Taylor, J. F., & Ripperdan, R. L. (2004). Flat-pebble conglomerate: its multiple origins and relationship to metre-scale depositional cycles. Sedimentology, 51(5), 973–996.

Nelson, S. T., Wood, M. J., Mayo, A. L., Tingey, D. G., & Eggett, D. (2005). Shoreline tufa and tufaglomerate from Pleistocene Lake Bonneville, Utah, USA: stable isotopic and mineralogical records of lake conditions, processes, and climate. Journal of Quaternary Science, 20(1), 3–19.

Oviatt, C. G., Currey, D. R., & Sack, D. (1992). Radiocarbon chronology of Lake Bonneville, eastern Great Basin, USA. Palaeogeography, Palaeoclimatology, Palaeoecology, 99(3–4), 225–241.

Pace, A., Bourillot, R., Bouton, A., Vennin, E., Galaup, S., Bundeleva, I., et al. (2016). Microbial and diagenetic steps leading to the mineralisation of Great Salt Lake microbialites. Scientific Reports, 6, 31495.

Payne, J. L., & Finnegan, S. (2006). Controls on marine animal biomass through geological time. Geobiology, 4(1), 1–10.

Payne, Jonathan L., Lehrmann, D. J., Wei, J., & Knoll, A. H. (2006). The pattern and timing of biotic recovery from the end-Permian extinction on the Great Bank of Guizhou, Guizhou Province, China. Palaios, 21(1), 63–85.

Phillips, J. D. (2009). Biological energy in landscape evolution. American Journal of Science, 309(4), 271–289.

Pruss, S. B., & Bottjer, D. J. (2004). Early Triassic trace fossils of the western United States and their implications for prolonged environmental stress from the end-Permian mass extinction. Palaios, 19(6), 551–564.

Pruss, S. B., Corsetti, F. A., & Bottjer, D. J. (2005). The unusual sedimentary rock record of the Early Triassic: a case study from the southwestern United States. Palaeogeography, Palaeoclimatology, Palaeoecology, 222(1–2), 33–52.

Rankey, E. C., & Reeder, S. L. (2009). Holocene ooids of Aitutaki Atoll, Cook Islands, South Pacific. Geology, 37(11), 971–974. https://doi.org/10.1130/G30332A.1

Rivers, J. M., Varghese, L., Yousif, R., Whitaker, F. F., Skeat, S. L., & Al-Shaikh, I. (2019). The Geochemistry of Qatar Coastal Waters and its Impact on Carbonate Sediment Chemistry and Early Marine Diagenesis. Journal of Sedimentary Research, 89(4), 293–309.

Rohweder, J., Rogala, J. T., Johnson, B. L., Anderson, D., Clark, S., Chamberlin, F., et al. (2012). Application of wind fetch and wave models for habitat rehabilitation and enhancement projects–2012 update. US Army Corps of Engineers, Contract Report.

Rohweder, J. J., Rogala, J. T., Johnson, B. L., Anderson, D., Clark, S., Chamberlin, F., & Runyon, K. (2008). Application of wind fetch and wave models for habitat rehabilitation and enhancement projects. Geological Survey (US).

Saltzman, M. R., Young, S. A., Kump, L. R., Gill, B. C., Lyons, T. W., & Runnegar, B. (2011). Pulse of atmospheric oxygen during the late Cambrian. Proceedings of the National Academy of Sciences, 108(10), 3876–3881.

Saltzman, M. R., Edwards, C. T., Adrain, J. M., & Westrop, S. R. (2015). Persistent oceanic anoxia and elevated extinction rates separate the Cambrian and Ordovician radiations. Geology, 43(9), 807–810.

Sanderson, D. J., & Donovan, R. N. (1974). The vertical packing of shells and stones on some recent beaches. Journal of Sedimentary Research, 44(3), 680–688.

Sepkoski, J. J. (1982). Flat-pebble conglomerates, storm deposits, and the Cambrian bottom fauna. In Cyclic and event stratification (pp. 371–385). Springer.

Shinn, E. A. (1969). Submarine lithification of Holocene carbonate sediments in the Persian Gulf. Sedimentology, 12(1-2), 109–144.

Shinn, E. A. (1983). Tidal flat environment. In Carbonate depositional environments (Vol. 33, pp. 171–210). American Association of Petroleum Geologists Tulsa.

Spencer, R. J., Eugster, H. P., Jones, B. F., & Rettig, S. L. (1985). Geochemistry of Great salt Lake, Utah I: hydrochemistry since 1850. Geochimica et Cosmochimica Acta, 49(3), 727–737.

Sun, Y., Joachimski, M. M., Wignall, P. B., Yan, C., Chen, Y., Jiang, H., et al. (2012). Lethally Hot Temperatures During the Early Triassic Greenhouse. Science, 338(6105), 366–370. https://doi.org/10.1126/science.1224126

Tarboton, D. (2017). Great Salt Lake Area Volume Data, HydroShare, http://www.hydroshare.org/resource/89125e9a3af544eab2479b7a974100ba

Thayer, C. W. (1979). Biological bulldozers and the evolution of marine benthic communities. Science, 203(4379), 458–461.

Thompson, R. S., Toolin, L. J., Forester, R. M., & Spencer, R. J. (1990). Accelerator-mass spectrometer (AMS) radiocarbon dating of Pleistocene lake sediments in the Great Basin. Palaeogeography, Palaeoclimatology, Palaeoecology, 78(3–4), 301–313.

Trower, E. J., Lamb, M. P., & Fischer, W. W. (2017). Experimental evidence that ooid size reflects a dynamic equilibrium between rapid precipitation and abrasion rates. Earth and Planetary Science Letters, 468, 112–118.

Trower, E. J., Cantine, M. D., Gomes, M. L., Grotzinger, J. P., Knoll, A. H., Lamb, M. P., et al. (2018). Active ooid growth driven by sediment transport in a high-energy shoal, Little Ambergris Cay, Turks and Caicos Islands. Journal of Sedimentary Research, 88(9), 1132–1151.

Twitchett, R. J. (1999). Palaeoenvironments and faunal recovery after the end-Permian mass extinction. Palaeogeography, Palaeoclimatology, Palaeoecology, 154(1–2), 27–37.

Utah Department of Water Quality (2014), 2012-2014 Final integrated report. Retrieved from (https://deq.utah.gov/legacy/programs/water-quality/monitoring-reporting/assessment/docs/2016/02feb/chapter_7_great_salt_lake_final20122014ir.pdf)

Vennin, E., Bouton, A., Bourillot, R., Pace, A., Roche, A., Brayard, A., et al. (2019). The lacustrine microbial carbonate factory of the successive Lake Bonneville and Great Salt Lake, Utah, USA. Sedimentology, 66(1), 165–204.

Vousdoukas, M. I., Velegrakis, A. F., & Plomaritis, T. A. (2007). Beachrock occurrence, characteristics, formation mechanisms and impacts. Earth-Science Reviews, 85(1–2), 23–46.

Walter, L. M., & Burton, E. A. (1990). Dissolution of recent platform carbonate sediments in marine pore fluids. American Journal of Science, 290(6), 601–643.

Walter, L. M., & Morse, J. W. (1984). Reactive surface area of skeletal carbonates during dissolution; effect of grain size. Journal of Sedimentary Research, 54(4), 1081–1090.

Wignall, P. B., & Twitchett, R. J. (1999). Unusual intraclastic limestones in Lower Triassic carbonates and their bearing on the aftermath of the end-Permian mass extinction. Sedimentology, 46(2), 303–316.

Williams, W. D., Boulton, A. J., & Taaffe, R. G. (1990). Salinity as a determinant of salt lake fauna: a question of scale. Hydrobiologia, 197(1), 257–266. https://doi.org/10.1007/BF00026955

Wright, V. P., & Cherns, L. (2016). Leaving no stone unturned: the feedback between increased biotic diversity and early diagenesis during the Ordovician. Journal of the Geological Society, 173(2), 241–244.

Wurtsbaugh, W. A. (1992). Food-web modification by an invertebrate predator in the Great Salt Lake (USA). Oecologia, 89(2), 168–175.

Wurtsbaugh, W. A. (2009). Biostromes, brine flies, birds and the bioaccumulation of selenium in Great Salt Lake, Utah. Natural Resources and Environmental Issues, 15(1), 2.

Wurtsbaugh, W. A., & Jones, E. F. (2012). The Great Salt Lake's deep brine layer and its importance for mercury bioaccumulation in brine shrimp (Artemia franciscana). Final Report to the Utah Division of Forestry Fire and State Lands, 1.

Yoo, K., Amundson, R., Heimsath, A. M., & Dietrich, W. E. (2005). Process-based model linking pocket gopher (Thomomys bottae) activity to sediment transport and soil thickness. Geology, 33(11), 917–920.

Zhong, S., & Mucci, A. (1989). Calcite and aragonite precipitation from seawater solutions of various salinities: Precipitation rates and overgrowth compositions. Chemical Geology, 78(3–4), 283–299.

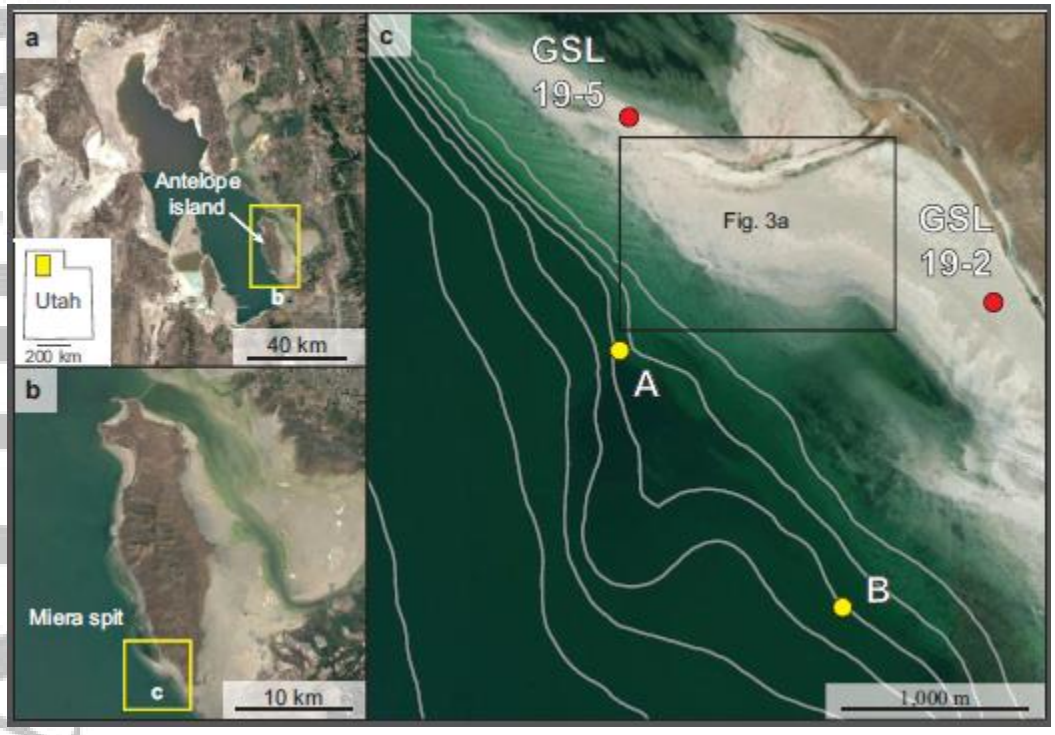

Figure 1. Google Earth (TM) imagery of the study location. a Overview of Great Salt Lake, UT. Antelope Island State Park is located within the southern Basin. b Inset of Antelope Island State Park. The light-colored rim around the island marks Holocene beaches, marshes, and deflation flats composed of carbonate sediments. c Inset of the study area near the southwest corner of Antelope Island. Contour lines show 1m changes in lake bathymetry calculated from the digital elevation model by Tarboton et al., (2017). Points GSL 19-2 and GSL 19-5 represent sample locations for unconsolidated sediments, while points A and B represent offshore sites evaluated in the wave models in Figures 2 and 7.

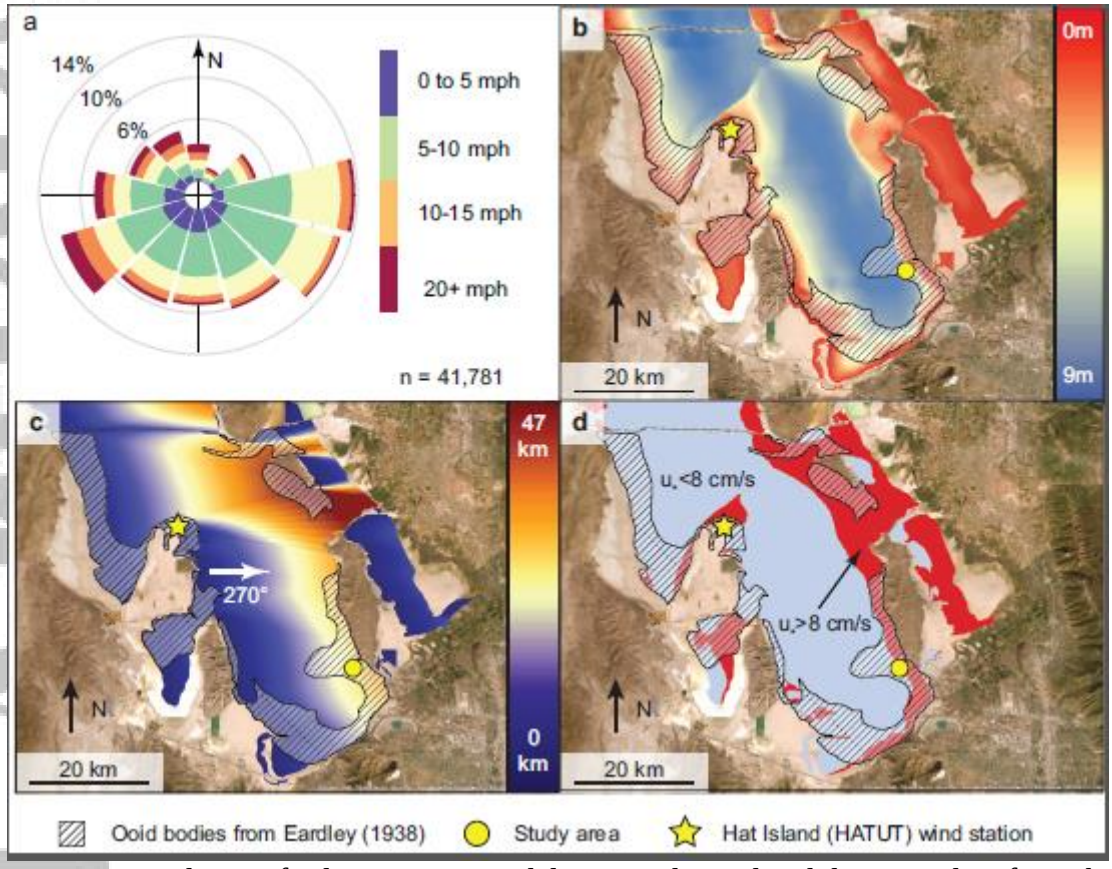

Figure 2. Data and maps for linear wave models. a Wind speed and direction data from the University of Utah's Mesowest database (Horel et al., 2002). Data were averaged over four-hour intervals and covered 1998-2020. b Bathymetry map calculated from a digital elevation model (Tarboton, 2017) at a lake level of 1279.15m. Ooid distributions (hatch pattern) are from Eardley (1938). c Fetch map calculated using the edges of the bathymetry map and a wind direction of 270°. d Example map of shear velocities calculated for 30 mph winds with a bearing of 270°.

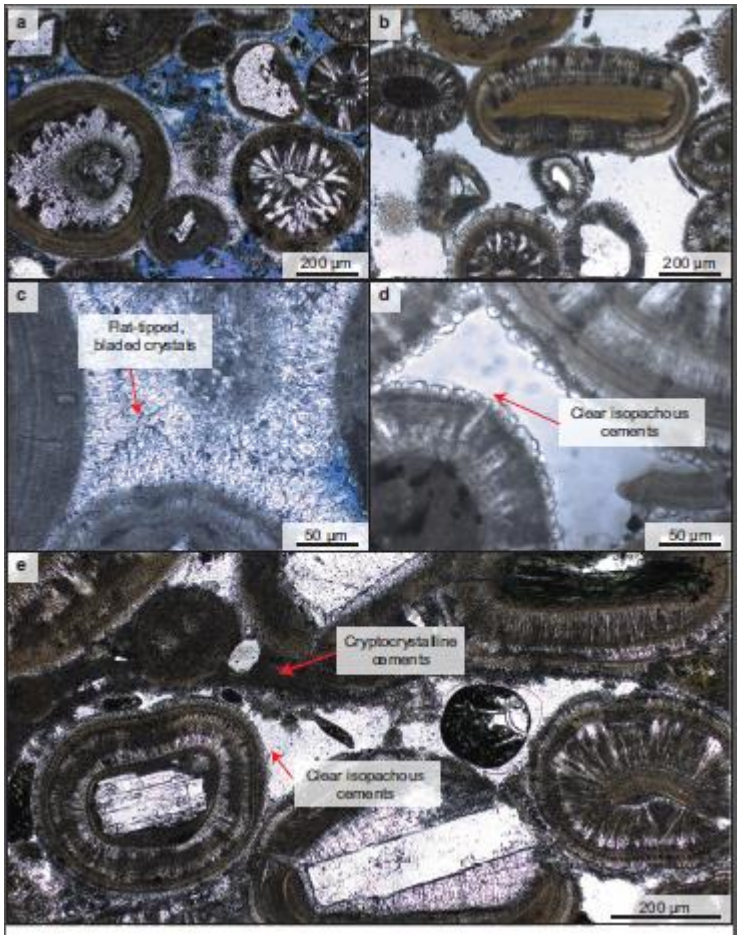

Figure 3. Photomicrographs of flat pebbles. **a** Sand-sized particles are dominantly ooids (coated grains) with both rinds of clear carbonate cement. Pores are filled with blue-stained epoxy. **b** Where cements are thinner, cement morphology is isopachous and subequant. Pores are filled with colorless epoxy. **c** Thicker cements display bladed crystals with flat tips, implying aragonite is the primary mineralogy. **d** Close up of subequant cements. The thinnest observed cements are ~5µm in length perpendicular to the ooid surface. **e** Early generation of micritic cement that develops near clast edges.

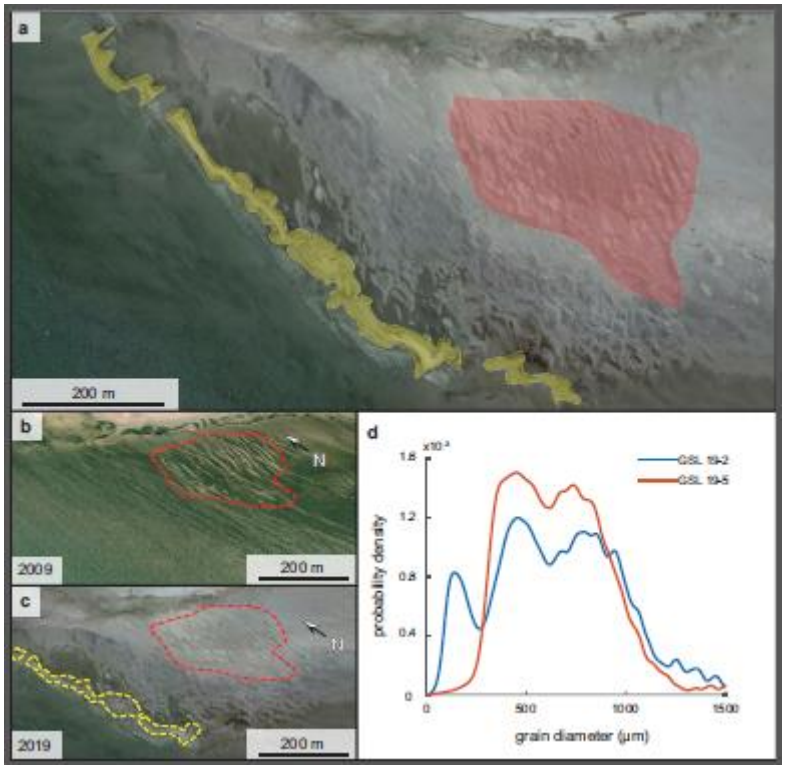

Figure 4. Large-scale sedimentary features near Miera spit and their relation to lake level history determined from satellite imagery and USGS-reported lake levels. aTwo classes of bedforms, including low-sinuosity to barchanoid bedforms (red) and shoreline-parallel ridges behind the current-day shoreline (yellow). b Satellite image from 2009 when the lake level was higher. The low-sinuosity bedforms are clearly visible adjacent to the spit. c Satellite imagery from 2019 showing lower overall lake levels. The low-sinuosity bedforms are exposed and the shoreline-parallel beach ridges have developed. d Distributions of intermediate axis diameter for ooid sand samples GSL19-2 and GSL19-5. Sample locations are shown in Fig. 1c.

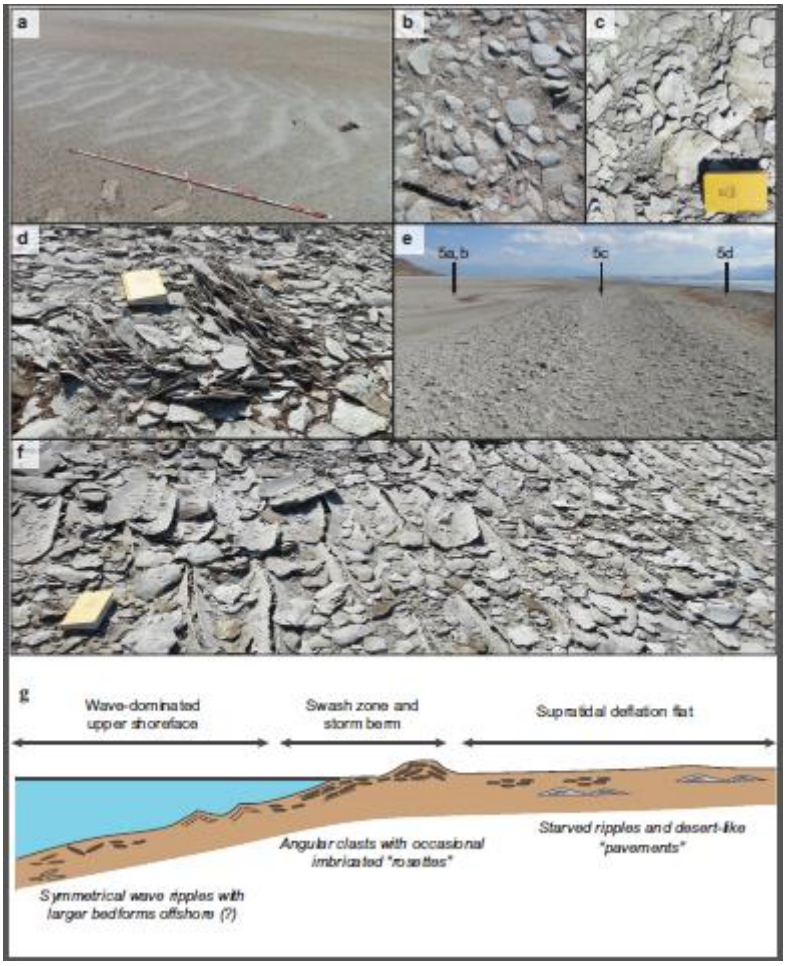

Figure 5. Facies exposed along the beach near Miera spit. **a** Starved ripple facies on top of a deflation surface. Light-colored, rippled sediment is slightly coarser than the darker underlying grainstones. **b** Rounded-to subrounded clasts of flat-pebble conglomerate. Clasts are smaller, rounder, and less frequent farther from the beach. **c** Larger, more angular clasts near that make up the shore-parallel ridges. **d** Imbricated "rosette" of flat-pebble conglomerate. These features are common products of storm-reworking in gravel shorelines (Sanderson & Donovan, 1974). **e** Low-relief ridge behind the shoreline, interpreted as a storm-berm. Annotations show the approximate locations of **a-d**. **f** Lithified, sharp-crested wave ripples in varying states of preservation. **g** Idealized facies model during a stable lake level.

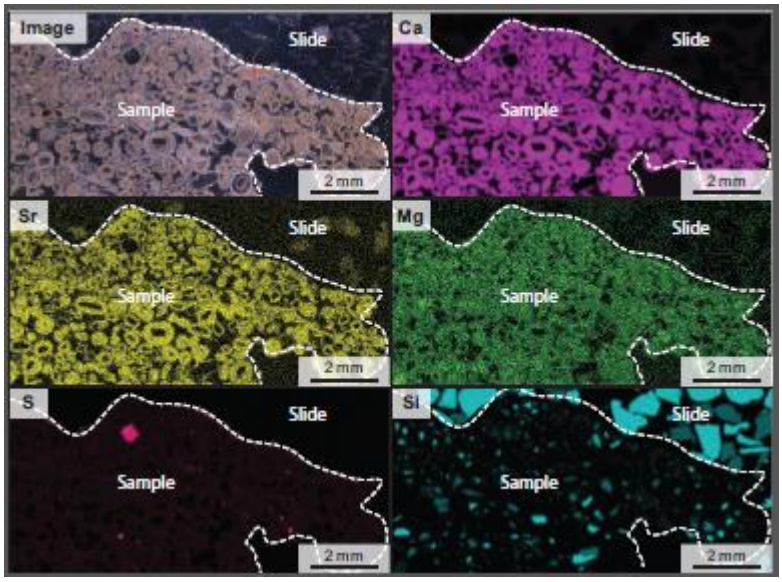

Figure 6. Maps of relative elemental abundances from μXRF. Both the oolitic cortices and interparticle cements are composed of calcium carbonate. Note that the low sulfur abundances between grains are inconsistent with sulfate evaporites (e.g., mirabolite). Spot size is approximately 20 microns.

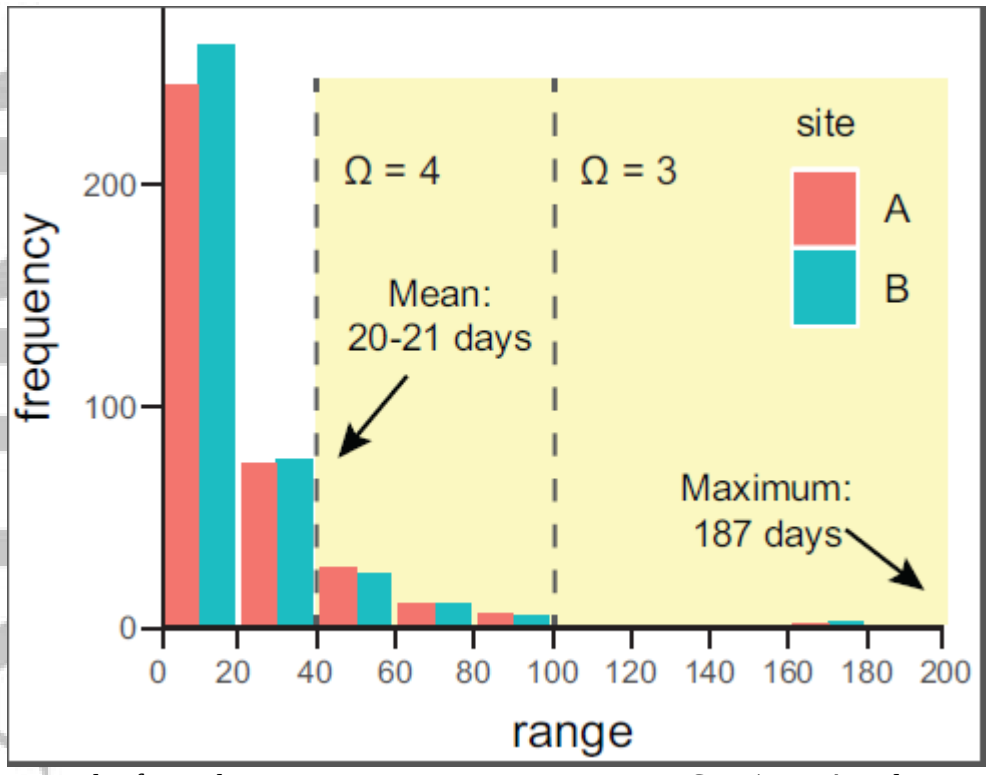

Figure 7. Length of time between transport events near Miera Spit (sites A and B in Fig. 1a). Periods were calculated by counting consecutive days for which shear velocity was below 8 cm/s at each site. The longest observed lag between transport events was 187 days, or approximately six months. Dashed lines show the amount of time it would take to precipitate 5µm-thick cements under a given saturation state. The timescales were calculated using Equation 2 with the constants from Table 1.

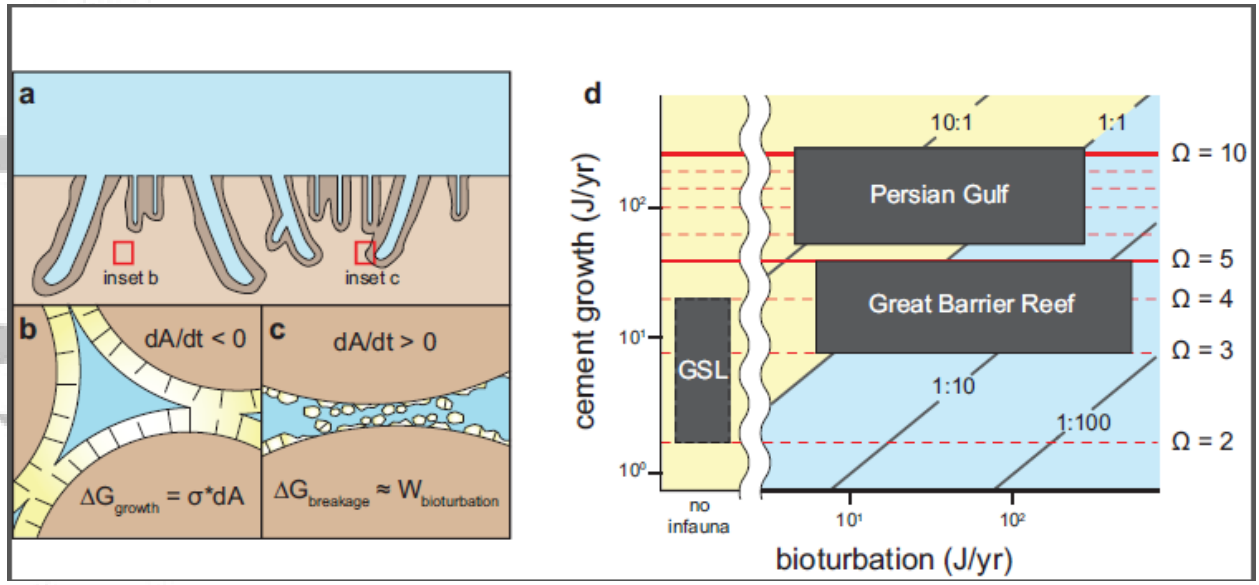

Figure 8. Competition between cementation and bioturbation. a Conceptual model for chemical and physical controls on substrate cohesion, focusing on the sediment-water interface. b During diagenesis, cement growth reduces the available surface area, reducing interfacial free energy but increasing sediment cohesion. c Burrowing organisms can fracture early cements and increase the surface area. This process opposes cementation and acts to keep the sediments loose. d Cross plot of changing interfacial work due to cement growth versus bioturbation for several modern settings. Notice that the variability in energy from bioturbation (x-axis) spans several orders of magnitude.

Table 1. Constants used to calculate energy change associated with bioturbation versus cementation (Eqns. 1-4, Figs. 7-8). Sources are (1) Zhong and Mucci (1989); (2) Trower et al. (2017); (3) Walter and Morse (1984); (4) Berner (1980); (5) Alongi (1989); (6) Coles and McCain (1990); (7) Gingras et al. (2008); (8) Dorgan et al. (2011); (9) Jiang et al. (2015); (10) Ingalls et al. (2020); (11) Rivers et al. (2019). SSA = specific surface area.

Parameter	value	source
k	0.113 mol m^2 yr^{-1}	1,2
n	2.26	1,2
M_{arag}	0.1 kg mol^{-1}	-
V_t	0.02 m^3	-
ϕ	0.4	-
ρ_{arag}	2850 kg m^3	
SSA	11.6 m2 kg^{-1}	3
A_i	397 m^{-2}	-
σ	0.08 J m^{-2}	4
Infaunal density near Great Barrier Reef	0.94-3.37 g m^{-2}	5
Infaunal density in the Persian Gulf	0.778-1.706 g m^{-2}	6
v	87.6-2540.4 m yr^{-1}	7
C	.064 J g-1 m^{-1}	8
$\Omega_{aragonite}$ for tropical seawater	3-5	9
$\Omega_{aragonite}$ for Great Salt Lake	2-4	10
$\Omega_{aragonite}$ for the Persian Gulf	5.5-10.7	11